

# Journal of Materials Chemistry A

Accepted Manuscript



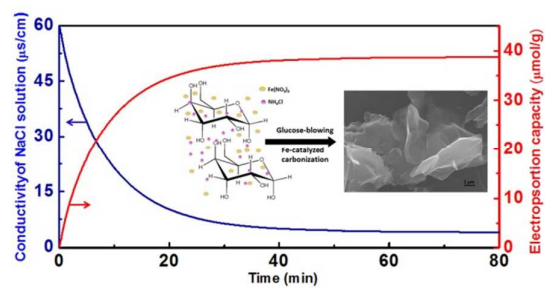
This is an *Accepted Manuscript*, which has been through the Royal Society of Chemistry peer review process and has been accepted for publication.

*Accepted Manuscripts* are published online shortly after acceptance, before technical editing, formatting and proof reading. Using this free service, authors can make their results available to the community, in citable form, before we publish the edited article. We will replace this *Accepted Manuscript* with the edited and formatted *Advance Article* as soon as it is available.

You can find more information about *Accepted Manuscripts* in the [Information for Authors](#).

Please note that technical editing may introduce minor changes to the text and/or graphics, which may alter content. The journal's standard [Terms & Conditions](#) and the [Ethical guidelines](#) still apply. In no event shall the Royal Society of Chemistry be held responsible for any errors or omissions in this *Accepted Manuscript* or any consequences arising from the use of any information it contains.

## TOC



Graphene-like carbon nanosheets prepared by a Fe-catalyzed glucose-blowing approach exhibit good performance for capacitive deionization.

## ARTICLE

# Graphene-like carbon nanosheets prepared by a Fe-catalyzed glucose-blowing method for capacitive deionization

Cite this: DOI: 10.1039/x0xx00000x

Hong Lei ‡, Tingting Yan ‡, Hui Wang, Liyi Shi, Jianping Zhang and Dengsong Zhang\*

Received 00th January 2012,

Accepted 00th January 2012

DOI: 10.1039/x0xx00000x

[www.rsc.org/](http://www.rsc.org/)

Capacitive deionization (CDI) is a new approach to produce fresh water from salted water sources. To achieve high CDI performance, we developed a facile method of fabricating graphene-like carbon nanosheets (GCNS) with a thickness of 2.4 nm by a Fe-catalyzed glucose-blowing approach. In this process, glucose is used as carbon precursors,  $\text{NH}_4\text{Cl}$  as blowing agents and Fe species as graphitization catalyst. The GCNS not only has a relatively large accessible surface area to accommodate more ions, but also has high graphitization to accelerate ion diffusion. The CDI performance of GCNS is evaluated by a batch mode electrosorptive experiment. The GCNS have higher electrosorptive capacity (38.62  $\mu\text{mol/L}$ ) compared with other carbon materials. It indicates that the GCNS is a novel and potential material for desalination.

## Introduction

As a serious global problem, the shortage of freshwater poses one of the greatest threats to humanity, due to the increasing demand for drinking water caused by the growing population<sup>1-3</sup>. Therefore, seawater desalination is one of the most pressing needs nowadays<sup>4,5</sup>. To solve this problem, a tremendous amount of effort has been made to develop new desalination methods<sup>6,7</sup>. Compared with traditional methods to remove salts from water such as reverse osmosis<sup>8-10</sup> and thermal processes<sup>11</sup>, capacitive deionization (CDI) was the least energy consuming and the most reversible deionization technology<sup>12,13</sup>. Nowadays CDI attracts great interest, because no chemicals are needed and no contaminants are produced during the environmentally-friendly process. The mechanism of CDI is based on the principle of electric double-layer capacitor (EDLC). Under the electric field, the oppositely charged CDI electrodes can electro-adsorb the salt ions from the NaCl aqueous solution and store them on the internal electrode surfaces. When the potential bias is removed, the adsorbed ions are released back to the bulk solution. According to the principle of EDLC, the performance of CDI largely depends on the internal structure and physical properties of the electrode materials, such as specific surface area, electrical conductivity, and porous structure<sup>14</sup>. To date, the materials for CDI electrodes have been extensively investigated by our research group and others<sup>14-16</sup>. With high electrical conductivity and large accessible surface area, carbon-based

materials had been considered as the favoured electrode materials for CDI, such as activated carbon, carbon aerogels<sup>17</sup>, carbon nanotubes<sup>18</sup>, porous carbon<sup>19</sup> and graphene<sup>20-22</sup>.

Two-dimensional (2D) carbon materials such as graphene<sup>23</sup> and graphene-like materials have stimulated great research interests in the past few years due to its high surface area, extraordinary conductivity, good chemical inertia and other unique properties. Graphene and graphene-like materials are considered as the superior candidates in a wide range of applications, such as supercapacitors<sup>24,25</sup>, solar cells<sup>26</sup>, light emitting diodes<sup>27</sup>, and batteries<sup>28,29</sup>. The synthetic methods of graphene and graphene-like materials include mechanical exfoliation<sup>30</sup>, reduction of chemically oxidized graphite<sup>31,32</sup>, thermal decomposition of  $\text{SiC}$ <sup>33</sup>, chemical vapor deposition<sup>34,35</sup>, exfoliation of graphite and graphite intercalated compounds<sup>36</sup>, solvothermal synthesis<sup>37</sup>. Unfortunately, all these methods are time-consuming, practically high-cost, relatively complicated and not environmentally-friendly<sup>38,39</sup>. Therefore, it is a critical challenge to exploit a facile and simple method to simultaneously fabricate graphene-like materials with high conductivity in large quantities.

It stimulates our interest to look for a cheap, abundant, commercially available, environmentally safe, and a sustainable material as a promising carbon source to produce graphene-like materials. As a potential carbon precursor material, glucose is widely distributed on the earth, and commonly used in daily life. Therefore, glucose becomes a widely used carbon source in the

production of activated carbon. Bando et al. had recently demonstrated that a 3D self-supported graphene prepared by a sugar-blowing approach based on a polymeric predecessor for supercapacitors<sup>40</sup>, but the high calcination temperature (1350 °C) was conducted, which is contradictory to the concept of energy saving. Shen et al. had reported a one-step ion-exchange/activation combination method to prepare a novel 3D hierarchical porous graphene-like material using a metal ion-exchange resin<sup>41</sup>, which is not environmentally-friendly.

the temperature normally required for the preparation of graphitic carbon<sup>44</sup>. The unique 2D ultrathin feature and partially graphitic characteristic of the GCNS are very favourable for the fast and steady transfer of the electrons and ions. Through the combined effects of gas-blowing and catalytic graphitization in the work, we found a new way to prepare the graphene-like nanosheets electrode with a high specific surface area and an enhanced electrical conductivity for CDI application.

## Experimental

### Preparation

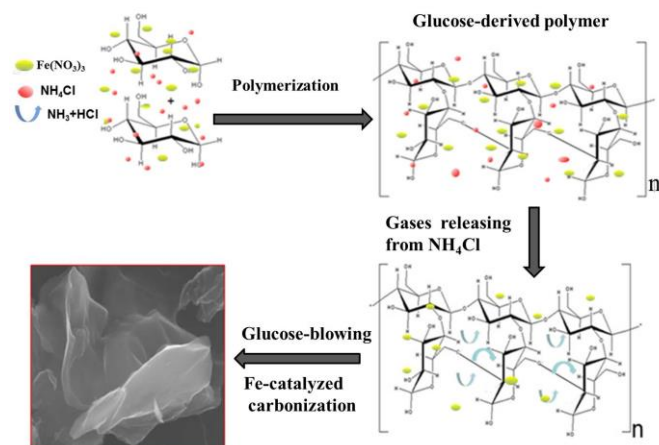
All chemicals were purchased from the Sinopharm Chemical Reagent Company. All these chemicals were of analytical grade and used without further purification, and deionized water was used in all of the process. Pure nitrogen was purchased from Shanghai Wugang Co. Ltd.

The GCNS materials with an ultrathin structure were synthesized through a facile glucose-blowing route by using glucose as carbon precursors,  $\text{NH}_4\text{Cl}$  as blowing agents and  $\text{Fe}(\text{NO}_3)_3 \cdot 9\text{H}_2\text{O}$  as graphitization catalyst precursors. In a typical synthesis, 5 g of glucose was mixed with 3.36 g of  $\text{Fe}(\text{NO}_3)_3 \cdot 9\text{H}_2\text{O}$  in deionized water (100 ml). Following an evaporation step at 48 °C for 2 h under stirring and then drying at 80 °C in a vacuum oven, the precursor was obtained. Subsequently, the precursor was mixed with  $\text{NH}_4\text{Cl}$  with the molar ratio of 1:1. After that, the process was carried out in a tubular furnace under a  $\text{N}_2$  atmosphere by heating the composite powders at a rate of 4 °C/min up to 950 °C for 3 h. Once cooled to room temperature, the obtained samples were treated with hot hydrochloric acid to dissolve the Fe species and then pure GCNS were obtained. For comparison, the carbon material with few nanosheet was produced in the same procedure without  $\text{Fe}(\text{NO}_3)_3 \cdot 9\text{H}_2\text{O}$ , which was denoted as C-1. The product of direct annealing glucose without  $\text{NH}_4\text{Cl}$  and  $\text{Fe}(\text{NO}_3)_3 \cdot 9\text{H}_2\text{O}$  was denoted as C-2.

### Characterization and electrochemical measurements

X-Ray diffraction (XRD) measurements were taken on a Rigaku D/MAX-RB X-ray diffractometer using Cu K $\alpha$  radiation (40 kV, 20 mA). The microstructure were observed by transmission electron microscopy (TEM, JEOL JEM-200CX) and field emission scanning electron microscopy (SEM, JEOL JSM-700F). To calculate the specific surface areas and the pore size distributions, the Brunauer–Emmett–Teller (BET) method was utilized with a Micromeritics ASAP 2010 analyzer. Atomic force microscopy (AFM, Multimode Nanoscope IIIa) method was utilized to calculate the thickness information of materials. The Fourier transform infrared spectroscopy (FT-IR) spectra of the samples were tested on AVATAR370 fourier transform infrared spectrometer. Raman spectra were recorded on a Raman system (INVIA) with confocal microscopy.

The electrochemical performance of the electrodes was evaluated by cyclic voltammetry (CV) using a CHI 660D, carries out in a three-compartment cell including a GCNS



**Scheme 1.** Illustration of the fabrication processes for GCNS.

Herein, we developed a facile and scalable synthesis strategy to fabricate graphene-like ultrathin carbon nanosheets by employing glucose as carbon precursor,  $\text{NH}_4\text{Cl}$  as blowing agent and Fe species as graphitization catalyst. The fabrication process of graphene-like carbon nanosheets (GCNS) is simply illustrated in Scheme 1. At the initial stage, the molten glucose was gradually polymerized and the glucose-derived polymers were formed.  $\text{Fe}(\text{NO}_3)_3 \cdot 9\text{H}_2\text{O}$  and  $\text{NH}_4\text{Cl}$  uniformly dispersed and absorbed in the glucose-derived polymers. Then, the chemically released gases ( $\text{HCl}$  and  $\text{NH}_3$ ) from  $\text{NH}_4\text{Cl}$  gradually blew the walls of the polymers to thinner and thinner. The carbon source can be graphitized at a lower carbonization temperature by the Fe-species catalyst. The graphene-like nanosheets with an ultrathin structure were formed through gas blowing process and Fe-catalyzed carbonization. Finally, the graphene-like nanosheets were immersed in hydrochloric acid to move the Fe-species and the graphene-like carbon nanosheets were obtained.

In this work, a low-cost and easily available resource, glucose was used as the carbon precursor. The Fe species embedded not only acted as a graphitization catalyst but also played a key role in the formation of 2D nanosheet structure<sup>38</sup>. The use of Fe species to prepare partially graphitic carbons via catalytic pyrolysis of carbon precursors is one of the commonly used methods<sup>42,43</sup>. The results demonstrated that GCNS with a high graphitization degree can be obtained at a low pyrolysis temperature of 950 °C, which was much lower than 2000 °C,

electrode, a piece of graphite, and a saturated calomel electrode, were used as the working, counter and reference electrodes, respectively. Here, the specific capacitances are obtained as the following equation:

$$C = \int IdV / 2v\Delta V/m \quad (1)$$

where  $C$  is the specific capacitance,  $I$  is the response current density,  $dV$  is the potential window,  $v$  is the potential scan rate and  $m$  is the mass of electrode material. The galvanostatic charge–discharge (GC) measurements were conducted on an automatic LAND battery test instrument to evaluate the charge–discharge performance in a 0.5M NaCl aqueous solution.

### Batch mode CDI experiments

The deionization performances of electrodes were evaluated by a batch mode CDI apparatus as described in our previous work<sup>4</sup>. The CDI electrode with a mass of 200 mg and a size of 60×70×0.2 mm were prepared as follows. The electrodes were manufactured by using active material, acetylene black and polytetrafluoroethylene with a weight ratio of 80: 10: 10 to form homogeneous slurries. During the preparation process, ethanol was added into the mixture to ensure it could be easily pressed onto graphite paper. At last, it was dried in a conventional oven at 110 °C overnight. Batch-mode includes two sided electrodes placed face to face and separated by an insulated spacer. The experiments were conducted in a continuously recycling system. In each experiment, a NaCl aqueous solution with an initial concentration of 30ppm (conductivity of 71μS/cm) and a total volume of 35 ml was supplied to the cell using a pump with a flow rate of 25 ml/min. The voltage between the two working electrodes is adjusted to 1.6 V. The concentration change of the solution was measured by connecting a conductivity meter at the outlet of the cell, where the solution was released. Herein, the electrosorptive capacity of the electrode materials was calculated according to the following equation:

$$Sc = (C_0 - C)V/m \quad (2)$$

where  $Sc$  is the electrosorptive capacity,  $C_0$  and  $C$  are the initial and final concentrations,  $V$  is the total volume of the NaCl aqueous solution, and  $m$  is the total mass of the electrodes.

## Results and discussion

### Material Characterization

The morphology of the GCNS was investigated by TEM and SEM. As presented in Fig. 1a, the GCNS displays a typical wrinkled and nearly transparent sheet-like structure with a few layers. The SEM image of GCNS in Fig. 1b shows a curly surface, where ultrathin layers can be observed in the whole sample. This morphology is similar to the reported graphene paper. Without Fe catalysts ( $\text{Fe}(\text{NO}_3)_3$ ) and blowing agents ( $\text{NH}_4\text{Cl}$ ), the graphene sheet-like structure cannot be observed in C-1 and C-2 (ESI, Fig. S1a and 1b). C-1 is mainly composed

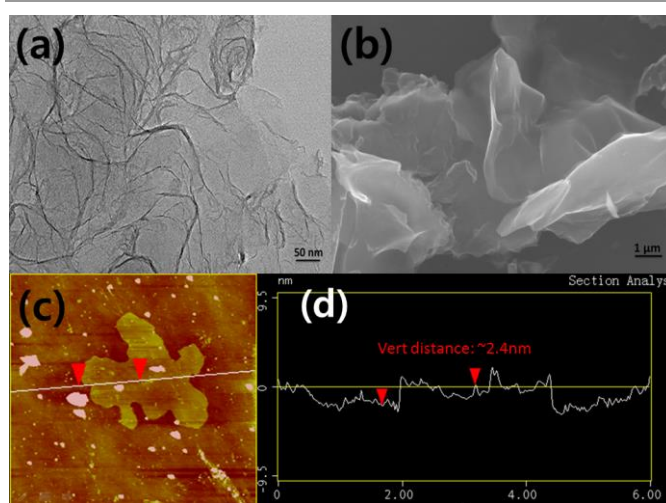


Fig.1 (a) TEM image, (b) SEM image, and (c,d) AFM images of the GCNS.

of large solids except with a few parts of nanosheets. C-2 shows severe agglomeration of particles rather than sheet-like structure. It indicates that the formation of graphene-like nanosheets should be employed the  $\text{NH}_4\text{Cl}$  and  $\text{Fe}(\text{NO}_3)_3$  simultaneously. It is deduced that the chemically released gases  $\text{HCl}$  and  $\text{NH}_3$  from  $\text{NH}_4\text{Cl}$  gradually blew the walls of the polymers to thinner and thinner; and subsequently the carbon source can be catalytically graphitized by the Fe species at the carbonization temperature. Generally, AFM is used to gain the insight into the thickness and morphology of the graphene-like nanosheets. AFM images (Fig. 1c) shows that the graphene-like material GCNS possesses a similar height with few-layered graphene. As it is presented in Fig.1d, the thickness of GCNS is approximately 2.4 nm which means seven graphitic layers. It indicates that the ultrathin graphene-like nanosheets are obtained successfully. This ultrathin structure of GCNS was also proved well through Tyndall effect of the GCNS solution (ESI, Fig. S2a). The specific surface area of GCNS is 220  $\text{m}^2/\text{g}$  according to nitrogen sorption-desorption isotherm (ESI, Fig. S2b).

The crystallised structures of the products GCNS, C-1 and C-2 were recorded by the wide-angle XRD. As shown in Fig.2a, two broad diffraction peaks at about 26° and 43° are observed, which belong to the typical (002) and (100) planes of graphitic materials. It is well known that the degree of graphitization can be evaluated by the height ratio of the (002) peak to the background, a relatively high value is usually associated with an improved degree of graphitization property<sup>36</sup>. Compared with those of C-1 and C-2, the XRD pattern of GCNS exhibits a relatively strong and sharp (002) peak, which indicates an increased degree of graphitization property of GCNS. The higher graphitization can increase the electrical conductivity, thus decrease the inner resistance of GCNS, which can be proved by the  $iR$  drop in the GC measurements in the following text.

The Raman spectroscopy is usually used to characterize the structural and electron properties of graphene-like materials. From the Raman spectra (Fig.2b) of GCNS, C-1 and C-2,

several peaks can be obviously observed at  $1342\text{ cm}^{-1}$  (D-mode),  $1571\text{ cm}^{-1}$  (G-mode),  $2698\text{ cm}^{-1}$  (2D-mode),  $2936\text{ cm}^{-1}$  (D+G mode). The 2D band peak is due to the highest optical branch phonons near the K point at the Brillouin Zone boundary<sup>45</sup>. It relates to the number of graphene layers for single-, bi- and few-layers. An asymmetric and broader 2D band indicates an increased graphene layers. Comparing with C-1 and C-2, an apparent sharp 2D band was observed for GCNS, which suggests that the GCNS is few graphitic layers. This is consistent with AFM results.

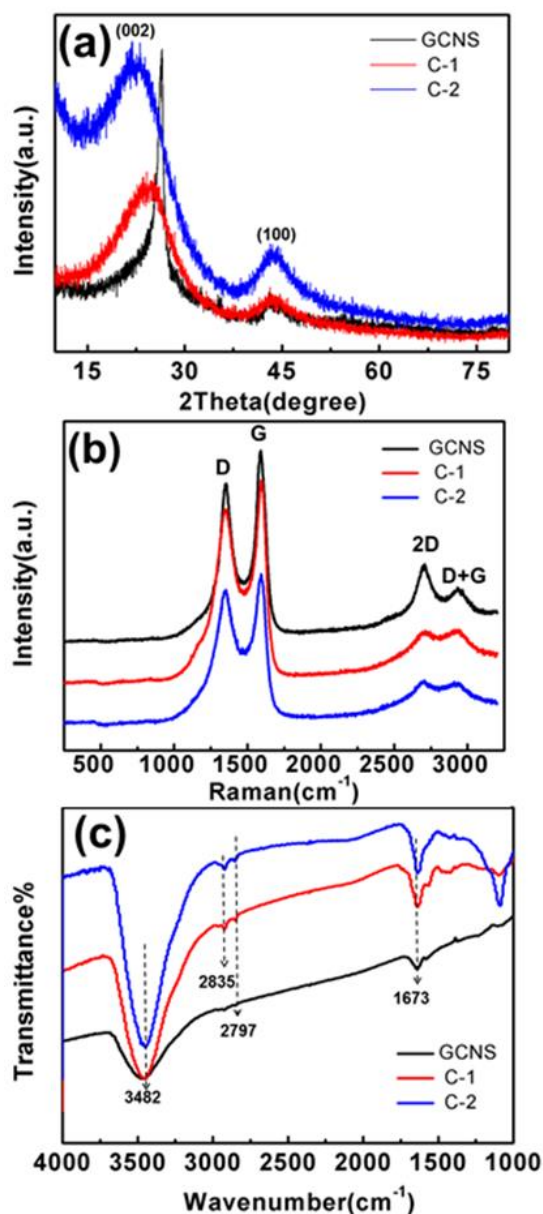


**Fig. 2** (a) XRD patterns, (b) Raman spectra, and (c) FT-IR spectra of GCNS, C-1 and C-2.

The surface functional groups of the GCNS, C-1 and C-2 can be confirmed by the FT-IR spectra. As shown in Fig. 2c, the characteristic FT-IR spectra of C-1 and C-2 are similar to that

of GCNS. The peaks at around  $3500\text{--}3400\text{ cm}^{-1}$  and  $1750\text{--}1630\text{ cm}^{-1}$  originates from  $\text{-OH}$  stretching mode and  $\text{C=O}$  skeletal vibration, respectively. Obviously, the peaks at around  $3500\text{--}3400$  and  $1750\text{--}1630\text{ cm}^{-1}$  are more pronounced on the C-1 and C-2 than the GCNS, which suggests that the content of the hydroxyl and carboxylic group on C-1 and C-2 is higher than that of the GCNS. It indicates ineffective removal of oxygen-containing groups of C-1 and C-2 without Fe-catalysts. The FT-IR spectra of GCNS and GH (prepared from hydrazine reduced graphene oxide) are quite similar (ESI, Fig.S3), indicating that the functional groups of GCNS are similar to those of GH. It means that the oxygen-containing groups on GCNS are effectively removed.

### Electrochemical behaviour

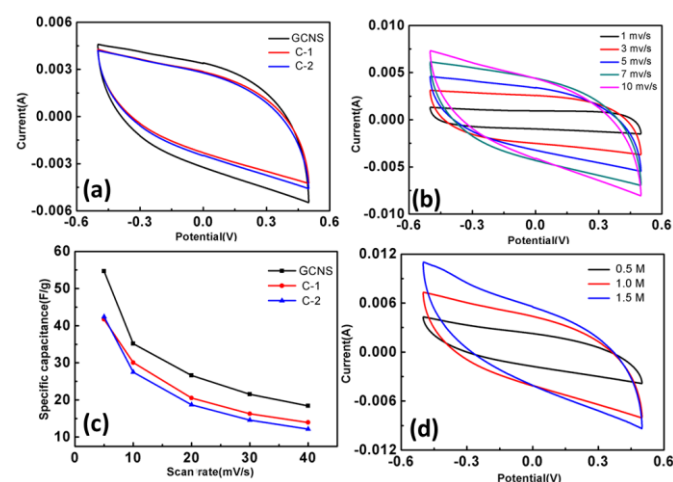


**Fig. 3** (a) CV curves of the GCNS, C-1, and C-2 electrodes at a scan rate of  $5\text{ mV/s}$  in a  $0.5\text{ M}$  NaCl aqueous solution; (b) the GCNS electrode at various scan rates in a  $0.5\text{ M}$  NaCl aqueous solution; (c) scan rates dependence of specific capacitance GCNS, C-1, and C-2 electrodes in  $0.5\text{ M}$  NaCl aqueous solution; and (d) comparative CV curves of GCNS electrodes at various NaCl concentrations at a scan rate of  $10\text{ mV/s}$ .

The CV analysis was carried out to investigate its electroadsorption behaviour. The capacitance examination on the samples was performed at room temperature. As shown in Fig. 3a, the CV profiles of the GCNS, C-1 and C-2 electrodes were obtained at a scan rate of  $5\text{ mV/s}$  in  $0.5\text{ M}$  NaCl aqueous solution with the potential window of  $-0.5$  to  $0.5\text{ V}$ . Apparently, no oxidation/reduction peaks appear in the chosen potential range, suggesting that the ions are mainly adsorbed on the electrode surface by forming an electric double layer capacitance due to the Coulombic interactions, rather than the electrochemical reduction/oxidation reactions<sup>11</sup>. The CV curves show a slight deviation of rectangular shapes, which are attributed to the inherent inner resistance and the polarization effect of electrodes<sup>15</sup>. Compared with C-1 and C-2, the CV curve of GCNS displays a nearly rectangular shape, indicating the charge current can reach the plateau quickly after reversing the potential sweep<sup>4</sup>. In other words, salty ions can quickly and effectively adsorb to and desorb from the electrode<sup>16</sup>. As an indicator of ion adsorption capacity, a higher closed area of the

CV curve is expected for an increased specific capacitance<sup>15</sup>. The specific capacitance of GCNS electrode is 54.68 F/g based on the calculation of CV curve at 10 mV/s, which is considerably larger than those of C-1 (42.39 F/g) and C-2 (41.72 F/g). For comparison, we also investigated the electrochemical capacitive performance of GCNS with GH (ESI, Fig.S4). As calculated, the species capacitance of the GH electrode is 43.94 F/g, and the value is smaller than that of the GCNS one (54.68 F/g). The high specific capacitance of the GCNS electrode results from the following reasons. (1) The GCNS electrode with high graphitization degree possesses a good electrical conductivity, which results in a low internal resistance. (2) The lateral dimension of the graphene-like sheets is continuous with a relatively ultrathin structure. It provides more active sites, such as edge-type sites to ensure more exposed surface readily accessible for the transport of salty solution<sup>46</sup>.

The CV curves of the GCNS electrode at different scan rate of 1-10 mV/s are presented in Fig.3b. There are no oxidation/reduction humps in the chosen range. Also, it shows symmetric shapes at any selected scan rate, which means rapid movement of ions into and out of GCNS electrode over a wide range of scan rates (1-10mV/s). In other words, Na<sup>+</sup> and Cl<sup>-</sup> ions can be fast and effectively adsorbed to and desorbed from the GCNS electrode. The CV curves present a relatively rectangular shape at the low scan rate such as 1 or 3 mV/s. However, when the scan rate increased to 10 mV/s, the curve shows a distorted from the typical rectangular shape, and turn to leaf-like shapes. This indicates that there is enough time for ions to diffuse and access to nearly all available surface of the GCNS at slower scan rates, leading to a better capacitive behaviour. However, when the scan rates are high, the salty ions do not have enough time to move and accumulate into the inner structure of the electrodes and lead to a relatively reduced accessible surface area. The plots corresponding to the specific capacitances of the electrodes versus scan rates are depicted in Fig.3c. Obviously, the specific capacitances tend to increase when the scan rate descends from 40 to 5 mV/s. It is noteworthy that the GCNS electrode always possesses the highest value at the chosen scan rates. The specific capacitance of GCNS is 18.39 F/g even at 40 mV/s, whereas C-1 and C-2 only possess the value of 13.95 F/g and 12.13 F/g, respectively. It means that the GCNS has the best EDLC performance among these three electrodes towards salty ions accumulation. In conclusion, the GCNS obtains the best electrical conductivity resulted from highest graphitization degree due to catalytic graphitization of Fe species<sup>47</sup>. Due to the good conductivity and more active sites of ultrathin graphene-like nanosheets, a large number of salty ions can be adsorbed on the surface of the GCNS electrode. The relatively good electrochemical performance of the GCNS endows it with great advantages towards water desalination compared to C-1 and C-2.

To investigate the effect of ion concentration on the electrosorption performance of the GCNS electrodes, the CV curves at a scan rate of 10 mV/s in 0.5, 1.0, and 1.5M NaCl aqueous media with the potential window of -0.5 to 0.5V are

shown in Fig.3d. Obviously, the area of the CV profiles increase with increasing the concentration of solution, indicating the accumulation of salt ions on the electrode can be effectively improved at a higher concentration. Meanwhile, the larger amount of ions can be adsorbed in the electric double layer region, resulting in an improved electronic conductivity. Therefore, more salt ions can be electrostatically adsorbed during the CDI process.

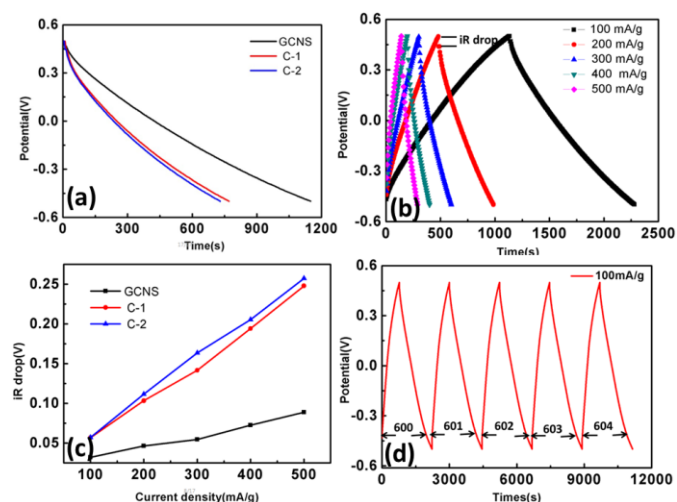


**Fig.4** (a) Galvanostatic discharges of the GCNS,C-1, and C-2 electrodes at 100 mA/g in 0.5 M NaCl aqueous solution; (b) typical GC curves of the GCNS electrode at various current densities in 0.5 M NaCl aqueous solution; (c) *iR* drops dependence of current densities of the GCNS, C-1, and C-2 electrodes; and (d) continuous GC curves of the GCNS, C-1, and C-2 electrodes with a current density of 100 mA/g in 0.5 M NaCl aqueous solution.

In order to further investigate the reversibility and stability performance of the GCNS, C-1 and C-2 electrodes, the galvanostatic discharge was performed in a potential window of -0.5 to 0.5V at the current density of 100 mA/g in 0.5 M NaCl aqueous solution. As shown in Fig. 4a, it can be observed that a nearly linear voltage profiles under a constant-current discharging, which is similar to a typical discharge profile of an EDLC. Moreover, the GCNS electrode shows the longest discharge time than those of C-1 and C-2 electrodes, indicating the higher specific capacitance. This is consistent with the CV results. We also performed the galvanostatic discharge of the GH in the same condition with GCNS. The discharge time of the GH electrode is slightly shorter than that of the GCNS one (ESI, Fig.S5). It is consistent with above-mentioned CV results, which means electrochemical performance of GCNS is better than the graphene prepared by the traditional routes. The galvanostatic charge/discharge curves of GCNS at a current load of 100-500 mA/g were shown in Fig. 4b. At various current densities, the GCNS electrode exhibits a typical triangular shape of ideal capacitor behaviour with fast charge propagation onto the electrode surface. In addition, the *iR* drop can be observed at the beginning of the discharge process, which is related to with the inner resistance of electrodes<sup>11</sup>. Therefore, we performed the variation tendency of *iR* drop against the current density. As seen in Fig.4c, the *iR* drop

increased nearly linearly with the increase of current densities, which was in consistent with the previously reported work<sup>4</sup>. Furthermore, the slope of the resulting diagram of  $iR$  drop is used to estimate the overall resistance of capacitor-like units. A lower slope in the profile means a lower overall resistance. The total internal resistance is one of the key factors for choice of electrode material. The GCNS electrode is suitable for CDI due to the lower inner resistance. Apart from the high specific capacitance, the reversibility and stability are also regarded as important indexes for high performance CDI electrodes. The cyclability of the GCNS electrode is investigated by the galvanostatic charge–discharge measurement at a constant current load of 100mA/g in 0.5 M NaCl aqueous solution. As presented in Fig.4d, the profile exhibits a classic triangular shape with symmetric and linear lines, representing typical EDLC behaviour rather than the Faradaic reaction. There is no charge/discharge decay been observed even after 600 cycles, indicating that this GCNS electrode displayed excellent stability and excellent cyclability. These crucial features ensure a long service life of GCNS for CDI application.

### CDI performance

To investigate the desalination behaviour of the fabricated electrodes, a series of batch mode CDI experiments were carried out in NaCl aqueous solution at 1.6V. Although the applied voltage (1.6 V) was higher than the Nernst potential for the breakdown of water (1.24 V), the intrinsic resistance of the electrode permits an overvoltage and thus no electrolysis happened in this voltage, which has been demonstrated by our research group as well as others<sup>7,48-52</sup>. The conductivity was tested due to its line relationship with the concentration. Fig. 5a displays the conductivity of NaCl aqueous solution variation along with the desalination time. Obviously, the conductivity of the solution decreases sharply at the beginning of the CDI processes, suggesting that  $\text{Na}^+$  and  $\text{Cl}^-$  are adsorbed onto the oppositely charged electrodes quickly. With the time going by, the conductivity decreases slowly, demonstrating that most of ions have been adsorbed onto the electrodes. Finally, the conductivity reaches to a stable value, indicating that electroadsorption equilibrium has achieved at the electrode. It is noted that the electrostatic repulsion between the same charged adsorbed ions prevent the constancy of electroadsorption. Moreover, as compared with C-1 and C-2 electrodes, the descending rate of conductivity for GCNS electrode is much faster, suggesting salty ions can be easily adsorbed at the electrode. As calculated, the electroadsorptive capacities of NaCl were 38.62  $\mu\text{mol/g}$ , 29.62 $\mu\text{mol/g}$  and 21.86 $\mu\text{mol/g}$  in 80 minutes for the GCNS, C-1 and C-2 electrodes, respectively. In other words, the GCNS electrode stores the most salty ions. Furthermore, we summarized the CDI performance of carbon based materials reported in the literature (ESI, Table S1); and apparently, the CDI capacity of the as-prepared GCNS is higher than those reported results.

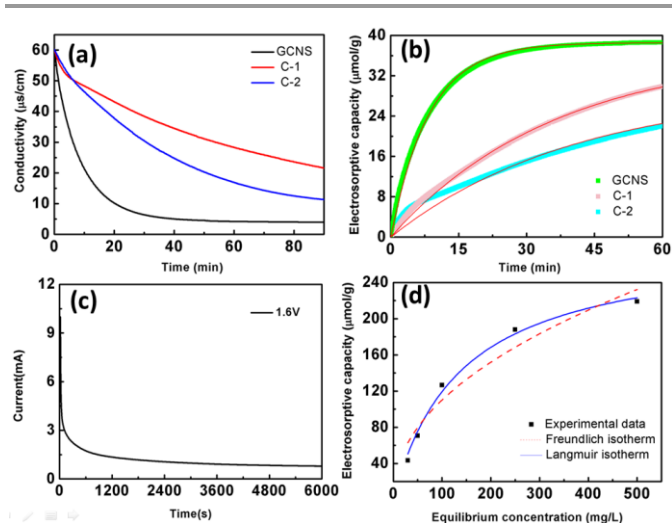


**Fig. 5** (a) The CDI profiles of the GCNS, C-1 and C-2 electrodes; (b) electroadsorption kinetics of ions onto the GCNS, C-1, C-2 electrodes; (c) current response of the GCNS and (d) experimental and fitting data by employing Langmuir and Freundlich isotherms for GCNS CDI.

Adsorption kinetics is often used to indicate the adsorption rate during the adsorption process.<sup>48</sup> The pseudo-first-order equation is employed to test the experimental data. The equation expressed as following equation:

$$\log(q_e - q) = \log q_e - kt/2.303 \quad (3)$$

where  $k$  ( $\text{min}^{-1}$ ) is the adsorption rate constant,  $q_e$  ( $\text{mg/g}$ ) and  $q$  ( $\text{mg/g}$ ) are the amounts of NaCl adsorbed at equilibrium and time  $t$  (min), respectively. The kinetics parameters can be obtained by fitting the experimental data using least square method. Fig. 5b presents the time-evolved desalination behaviours of GCNS, C-1 and C-2 materials in 30 mg/L NaCl solution. Obviously, the electroadsorption of NaCl for GCNS can quickly reach equilibrium, which is much faster than those of C-1 and C-2. The experimental data of all three electrodes are found to be in agreement with the pseudo-first-order law based on the regression coefficient  $r^2 > 0.98$ . The corresponding rate constants are 0.119, 0.028 and 0.024  $\text{min}^{-1}$  respectively as shown in Table 1. The result shows the GCNS has the fastest electroadsorption rate.

**Table 1** Parameters determined from isotherms of GCNS, C-1 and C-2 in CDI.

	$k$ ( $\text{min}^{-1}$ )	$R^2$
GCNS	0.119	0.997
C-1	0.028	0.999
C-2	0.024	0.981

Charge efficiency  $\lambda$  is an important tool to examine the dynamic process of electroadsorption<sup>16</sup>. In principle, it is defined as the ratio of electroadsorption capacity to charge and thereby it is much useful to evaluate how much the electrical voltage contributes to the adsorption and is calculated according to the following equation:

$$\lambda = (F * F) / \Sigma \quad (4)$$

where  $F$  is the Faraday constant (96485 C/mol),  $\Gamma$  is the electrosorption capacity with units of mol/g and  $\Sigma$  (charge, C/g) is obtained by integrating the corresponding current. As presented in Fig.5c, the calculated  $\alpha$  of the GCNS is about 0.47, which is higher than those of C-1 (0.34) and C-2 (0.30). It indicates that GCNS is the best material for enhancing the charge efficiency. This is attributed to the more active sites provided by ultrathin nanosheets and lower inner resistance of the GCNS electrodes. All of these features indicate that the GCNS is an excellent candidate electrode material for CDI application.

**Table 2** The determined parameters and regression coefficients  $R^2$ ,  $K_L$  and  $K_F$  of Langmuir and Freundlich isotherms of GCNS at 298K.

Isotherm	Parameter	GCNS
Langmuir	$q_m$	224.904
	$K_L$	0.007
	$R^2$	0.989
Freundlich	$K_F$	12.98
	$1/n$	2.16
	$R^2$	0.9223

The electrosorption isotherm is regarded as one of the most important data to describe the mechanism of the adsorption<sup>3</sup>. The electrosorption isotherms of GCNS electrode were obtained by altering the initial NaCl concentrations to investigate the electrosorption behaviour. The experimental data can be fitted by applying the Langmuir (Eq.5) and Freundlich models (Eq.6), which usually simulate the aqueous-phase adsorption. The Langmuir Eq.5 and Freundlich Eq.6 expressed as following:

$$q_e = q_m k_L C_e / (1 + k_L C_e) \quad (5)$$

$$q_e = k_F C_e^{1/n} \quad (6)$$

where  $q_e$  is (mg/g) is the amount of removed NaCl,  $C_e$  is the equilibrium concentration (mg/L), and  $q_m$  (mg/g) is the maximum removal capacity corresponding to complete monolayer coverage,  $n$  is an empirical constants.  $K_L$  and  $K_F$  are the Langmuir constant and the Freundlich constant, respectively. Fig.5d shows the removal capacities increase with the concentration and then reach a plateau. The parameter of Langmuir and Freundlich model and regression coefficients are listed in Table 2. From the regression coefficient  $R^2$ , the Langmuir isotherm fits the experimental data of GCNS better than the Freundlich isotherm. It is indicate that the monolayer absorption is the main adsorption mechanism during electrosorption process.

## Conclusions

In conclusion, we developed a cost-effective and simple method to effectively synthesize the well-defined GCNS materials with a thickness of ~2.4 nm. By using glucose as carbon precursor,  $NH_4Cl$  as blowing agent, and Fe species as graphitization catalyst, we provide a universal pathway to

obtain the ultrathin carbon material. The use of Fe-catalyst and glucose-blowing way stands out of many previous routes for making graphene-like nanosheets. The superior behaviour of GCNS is attributed to the following reasons. Firstly, the good electrical conductivity owing to the high graphitization degree of GCNS promotes the electron transport during the charge-discharge process. Secondly, the ultrathin graphene-like nanosheets could provide more active site for CDI application. So it provides more ion absorbed site. Furthermore, the CDI performance investigated by the batch-mode apparatus demonstrated that the GCNS electrode has a higher deionization capacity than mostly reported carbon-based materials. Therefore, we provide a promising material for desalination of salt water by the CDI process.

## Acknowledgements

The authors acknowledge the support of the Science and Technology Commission of Shanghai Municipality (13NM1401200), the National Basic Research Program of China (2014CB660803), the Shanghai Municipal Education Commission (14ZZ097) and the Shanghai Special Foundation for Cultivation of Youth Teacher from Universities (B.37-0407-11-002). The authors would like to thank Mr W. J. Yu from the Analysis and Test Center of SHU for help with the TEM measurements. The author also gratefully acknowledge Mr Christopher Sole and Tzu-Ho Wu from University of Liverpool for help with polishing the English writing.

## Notes and references

Research Center of Nano Science and Technology, Shanghai University, Shanghai 200444, China. E-mail: dszhang@shu.edu.cn; Fax: +86 21 66136079; Tel: +86 021 66136081

†Electronic Supplementary Information (ESI) available: TEM images of C-1 and C-2; Tyndall effect of the GCNS solution, and Nitrogen sorption isotherm and BJH pore size distribution for GCNS; The FT-IR spectra of GCNS and GH; CV curves of the GCNS, and GH electrodes at a scan rate of 5 mV/s; Galvanostatic discharges of the GCNS, and GH electrodes at 100 mA/g; The CDI capacity ( $Q_m$ ) of different electrode materials. See DOI: 10.1039/b000000x/

‡These authors contributed equally to this work.

- (1) H. Y. Yang, Z. J. Han, S. F. Yu, K. L. Pey, K. Ostrikov, R. Karnik, *Nat. Commun.*, 2013, **4**, 2220-2227.
- (2) Z. Y. Yang, L. J. Jin, G. Q. Lu, Q. Q. Xiao, Y. X. Zhang, L. Jing, X. X. Zhang, Y. M. Yan, K. N. Sun, *Adv. Funct. Mater.*, 2014, **24**, 3917-3925.
- (3) H. B. Li, L. D. Zou, L. K. Pan, Z. Sun, *Environ. Sci. Technol.*, 2010, **44**, 8692-8697.
- (4) X. R. Wen, D. S. Zhang, L. Y. Shi, T. T. Yan, H. Wang, J. P. Zhang, *J. Mater. Chem.*, 2012, **22**, 23835-23844.
- (5) G. Wang, Q. Dong, Z. Ling, C. Pan, C. Yu, J. H. Qiu, *J. Mater. Chem.*, 2012, **22**, 21819-21823.
- (6) M. Pasta, C. D. Wessells, Y. Cui, F. La Mantia, *Nano lett.*, 2012, **12**, 839-843.

- (7) P. Dlugolecki, A. van der Wal, *Environ. Sci. Technol.*, 2013, **47**, 4904-4910.
- (8) E. N. Wang, R. Karnik, *Nat. Nanotech.*, 2012, **7**, 552-554.
- (9) B. E. Logan, M. Elimelech, *Nature*, 2012, **488**, 313-319.
- (10) A. Altaee, A. Mabrouk, K. Bourouni, *Desalination*, 2013, **326**, 19-29.
- (11) R. Zhao, P. M. Biesheuvel, A. van der Wal, *Energy Environ. Sci.*, 2012, **5**, 9520-9527.
- (12) L. D. Zou, L.X. Li, H.H. Song, G. Morris, *Water Res.*, 2008, **42**, 2340-2348.
- (13) D. S. Zhang, T. T. Yan, L. Y. Shi, Z. Peng, X. R. Wen, J. P. Zhang, *J. Mater. Chem.*, 2012, **22**, 14696-14704.
- (14) S. Jeon, H. Park, J. Yeo, S. Yang, C. H. Cho, M. H. Han, D. K. Kim, *Energy Environ. Sci.*, 2013, **6**, 1471-1475.
- (15) H. Wang, L. Y. Shi, T. T. Yan, J. P. Zhang, Q. D. Zhong, D. S. Zhang, *J. Mater. Chem. A*, 2014, **2**, 4739-4750.
- (16) H. B. Li, S. Liang, J. Li, L. J. He, *J. Mater. Chem. A*, 2013, **1**, 6335-6341.
- (17) Y. Liu, C. Y. Nie, L. K. Pan, X. T. Xu, Z. Sun, D. H. C. Chua, *Inorg. Chem. Front.*, 2014, **1**, 249-255.
- (18) L. Wang, M. Wang, Z. H. Huang, T. Cui, X. Gui, F. Kang, K. Wang, D. Wu, *J. Mater. Chem.*, 2011, **21**, 18295-18299.
- (19) R. T. Mayes, C. Tsouris, J. O. Kiggans Jr, S. M. Mahurin, D. W. DePaoli, S. Dai, *J. Mater. Chem.*, 2010, **20**, 8674-8678.
- (20) H. Wang, D. S. Zhang, T. T. Yan, X. R. Wen, L. Y. Shi, J. P. Zhang, *J. Mater. Chem.*, 2012, **22**, 23745-23748.
- (21) H. J. Yin, S. L. Zhao, J. W. Wan, H. J. Tang, L. Chang, L. C. He, H. J. Zhao, Y. Gao, Z. Y. Tang, *Adv. Mater.*, 2013, **25**, 6270-6276.
- (22) B. H. Li, F. Zaviska, S. Liang, J. Li, L. J. He, H. Y. Yang, *J. Mater. Chem. A*, 2014, **2**, 3484-3491.
- (24) Y. Zhu, S. Murali, M. D. Stoller, K. J. Ganesh, W. Cai, P. J. Ferreira, A. Pirkle, R. M. Wallace, K. A. Cychosz, M. Thommes, D. Su, E. A. Stach, R. S. Ruoff, *Science*, 2011, **332**, 1537-1541.
- (24) C. X. Guo, C. M. Li, *Energy Environ. Sci.*, 2011, **4**, 4504-4507
- (25) R. B. Rakhi, W. Chen, D. Cha, H. N. Alshareef, *J. Mater. Chem.*, 2011, **21**, 16197-16204.
- (26) Y. Wang, S. W. Tong, X. F. Xu, B. Ozyilmaz, K. P. Loh, *Adv. Mater.*, 2011, **23**, 1514-1518.
- (27) C. H. Lee, Y. J. Kim, Y. J. Hong, S. R. Jeon, S. Bae, B. H. Hong, G. C. Yi, *Adv. Mater.*, 2011, **23**, 4614-4619.
- (28) S. S. Li, Y. H. Luo, W. Lv, W. J. Yu, S. Wu, P. X. Hou, Q. H. Yang, Q. B. Meng, C. Liu, H. M. Cheng, *Adv. Energy Mater.*, 2011, **1**, 486-490.
- (29) H. D. Liu, P. Gao, J. H. Fang, G. Yang, *Chem. Commun.*, 2011, **47**, 9110-9112.
- (30) K. S. Novoselov, A. K. Geim, S. V. Morozov, D. Jiang, Y. Zhang, S. V. Dubonos, I. V. Grigorieva, A. A. Firsov, *Science*, 2004, **306**, 666-669.
- (31) S. Stankovich, D. A. Dikin, G. H. Dommett, K. M. Kohlhaas, E. J. Zimney, E. A. Stach, R. D. Piner, S. T. Nguyen, R. S. Ruoff, *Nature*, 2006, **442**, 282-286.
- (32) S.X. Wu, Z. Y. Yin, Q. Y. He, G. Lu, X. Z. Zhou, H. Zhang, *Mater. Chem.*, 2011, **21**, 3467-3470.
- (33) P. Sutter, *Nat. Mater.*, 2009, **8**, 171-172.
- (34) L. B. Gao, W. C. Ren, H. L. Xu, L. Jin, Z. X. Wang, T. Ma, L. P. Ma, Z. Y. Zhang, Q. Fu, L. M. Peng, X. H. Bao, H. M. Cheng, *Nat. Commun.*, 2012, **3**, 699-705.
- (35) X. S. Li, W. W. Cai, J. H. An, S. Kim, J. Nah, D. X. Yang, R. Piner, A. Velamakanni, I. Jung, E. Tutuc, S. K. Banerjee, L. Colombo, R. S. Ruoff, *Science*, 2009, **324**, 1312-1314.
- (36) X. L. Li, X. R. Wang, L. Zhang, S. Lee, H. J. Dai, *Science*, 2008, **319**, 1229-1232.
- (37) M. Choucair, P. Thordarson, J. A. Stride, *Nat. Nanotechnol.*, 2009, **4**, 30-33.
- (38) L. Sun, C. G. Tian, M. T. Li, X. Y. Meng, L. Wang, R. H. Wang, J. Yin, H. G. Fu, *J. Mater. Chem. A*, 2013, **1**, 6462-6470.
- (39) B. B. Wang, K. Ostrikov, T. van der Laan, K. Zheng, J. J. Wang, Y. P. Yan, X. J. Quan, *J. Mater. Chem. C*, 2013, **1**, 7703-7708.
- (40) X. B. Wang, Y. J. Zhang, C. Y. Zhi, X. Wang, D. M. Tang, Y. B. Xu, Q. H. Weng, X. F. Jiang, M. Mitome, D. Golberg, Y. Bando, *Nat. Commun.*, 2013, **4**, 2905-2912.
- (41) Y. Y. Li, Z. H. Li, P. K. Shen, *Adv. Mater.*, 2013, **25**, 2474-2480.
- (42) A. H. Lu, W. C. Li, G. P. Hao, B. Spliethoff, H. J. Bongard, B. B. Schaack, F. Schuth, *Angew. Chem. Int. Ed.*, 2010, **49**, 1615-1618.
- (43) A. H. Lu, W. C. Li, E. L. Salabas, B. Spliethoff, F. Schuth, *Chem. Mater.*, 2006, 2086-2094.
- (44) L. Dong, Z. X. Chen, D. Yang, H. B. Lu, *RSC Adv.*, 2013, **3**, 21183-21191.
- (45) Y. Shen, A. C. Lua, *Sci. Rep.*, 2013, **3**, 3037-3042.
- (46) G. Srinivas, Y. W. Zhu, R. Piner, N. Skipper, M. Ellerby, R. Ruoff, *Carbon*, 2010, **48**, 630-635.
- (47) L. Chen, Z. Y. Wang, C. N. He, N. Q. Zhao, C. S. Shi, E. Z. Liu, J. J. Li, *ACS Appl. Mater. Interf.*, 2013, **5**, 9537-9545.
- (48) B. H. Li, T. Lu, L. K. Pan, Y. P. Zhang, Z. Sun, *J. Mater. Chem.*, 2009, **19**, 6773-6779.
- (49) H. Wang, D. S. Zhang, T. T. Yan, X. R. Wen, J. P. Zhang, L. Y. Shi, Q. D. Zhong, *J. Mater. Chem. A*, 2013, **1**, 11778-11789.
- (50) Q. Dong, G. Wang, B. Q. Qian, C. Hu, Y. W. Wang, J. S. Qiu, *Electrochim. Acta*, 2014, **137**, 388-394.
- (51) G. Wang, B. Q. Qian, Q. Dong, J. Y. Yang, Z. B. Zhao, J. S. Qiu, *Sep. Purif. Technol.*, 2013, **103**, 216-221.
- (52) G. Wang, C. Pan, L. P. Wang, Q. Dong, C. Yu, Z. B. Zhao, J. S. Qiu, *Electrochim. Acta*, 2012, **69**, 65-70.